Solid-state nuclear magnetic resonance in the rotating tilted frame

Nicole M. Trease and Philip J. Grandinetti[a)]
Department of Chemistry, Ohio State University, Columbus, Ohio 43210, USA

(Received 24 September 2007; accepted 17 December 2007; published online 4 February 2008)

Recent methodological advances have made it possible to measure fine structure on the order of a few hertz in the nuclear magnetic resonance (NMR) spectra of quadrupolar nuclei in polycrystalline samples. Since quadrupolar couplings are often a significant fraction of the Zeeman coupling, a complete analysis of such experimental spectra requires a theoretical treatment beyond first-order. For multiple pulse NMR experiments, which may include sample rotation, the traditional density matrix approaches for treating higher-order effects suffer from the constraint that undesired fast oscillations (i.e., multiples of the Zeeman frequency), which arise from allowed overtone transitions, can only be eliminated in numerical simulations by employing sampling rates greater than $2I$ times the Zeeman frequency. Here, we present a general theoretical approach for arbitrary spin I that implements an analytical "filtering" of undesired fast oscillations in the rotating tilted frame, while still performing an exact diagonalization. Alternatively, this approach can be applied using a perturbation expansion for the eigenvalues and eigenstates, such that arbitrary levels of theory can be explored. The only constraint in this approach is that the Zeeman interaction remains the dominant interaction. Using this theoretical framework, numerical simulations can be implemented without the need for a high sampling rate of observables and with significantly reduced computation times. Additionally, this approach provides a general procedure for focusing on the excitation and detection of both fundamental and overtone transitions. Using this approach we explore higher-order effects on a number of sensitivity and resolution issues with NMR of quadrupolar nuclei. © *2008 American Institute of Physics*. [DOI: 10.1063/1.2833580]

I. INTRODUCTION

Numerous developments in recent years for improving the resolution and sensitivity of quadrupolar nuclei have transformed many nuclear magnetic resonance (NMR) active nuclei from esoteric into routine probes of structure in solids. Earlier difficulties stemmed from the large quadrupolar interactions, which are often many orders of magnitude stronger than other internal spin interactions (e.g., chemical shift, J-couplings, dipolar couplings, etc.), and sometimes even stronger than the Zeeman interaction. The key to designing methods for improving resolution, such as double rotation (DOR),[1,2] two-dimensional (2D) dynamic-angle spinning (DAS),[2,3] 2D multiple-quantum magic-angle spinning (MQ-MAS),[4,5] and 2D satellite transition magic-angle spinning (ST-MAS),[6] was a careful analysis of the perturbation expansion to second-order for the NMR transition frequency. With the enormous success of these methods and related theoretical analyses there has been an explosion of solid-state NMR studies using quadrupolar nuclei in a variety of materials. Over the years, a few researchers have found subtle, and sometimes not so subtle,[7–9] effects in NMR spectra of quadrupolar nuclei that require theoretical analysis beyond the second-order perturbation theory. Understanding how these higher-order effects manifest themselves in solid-state NMR spectra is becoming increasingly important as researchers push the limits of resolution and sensitivity of quadrupolar nuclei to measure and exploit J-couplings[10,11] and second-order dipolar-quadrupolar[12,13] and chemical shift anisotropy-quadrupolar[14] cross terms in the spectra of samples containing quadrupolar nuclei. Compared to the symmetric multiple quantum and central transitions, higher-order effects are particularly prevalent in the nonsymmetric (satellite) transitions of quadrupolar nuclei.[8,14,15] With the increased use of ST-MAS, as well as recent success with indirect detection of ^{14}N magic-angle spinning in solids,[16–19] a general theoretical approach is clearly needed for a more complete analysis of experimental NMR spectra involving quadrupolar nuclei.

Generally, there can be up to $I(2I+1)$ allowed transitions for a single spin I, and, if one coupling dominates, the highest transition frequencies could be as large as $2I$ times that coupling. In the limit where the Zeeman coupling is infinitely larger than all other couplings, there will be only $2I$ allowed transitions, all having frequencies near the Larmor frequency ω_0. In this case, a transformation of the density operator into a frame rotating at a frequency near ω_0 leaves only the slower oscillations from the remaining "truncated" couplings. In contrast, when the Zeeman coupling is finite compared to the remaining couplings, then one has to allow for all $I(2I+1)$ transitions. If the Zeeman coupling remains the largest, then it still can be sensible to employ a rotating frame transformation, however, this transformation no longer guarantees that all fast oscillations are eliminated and only slow oscillations remain in the rotating frame density operator. Thus, to prevent undesired fast oscillations from aliasing

[a)]URL: http://www.grandinetti.org.

when calculating observables in the rotating frame one is forced to use a sample rate that exceeds the highest allowed transition frequencies.[20]

Here, we expand on an idea, first described by Goldman *et al.*,[20] where the the Hamiltonian and observable operators are expanded in terms of irreducible spherical tensor operators and Δm_I (or the harmonics of the fundamental Zeeman frequency). This approach can be employed, as shown by Goldman *et al.*,[20] using either static perturbation theory or, as shown here, using exact numerical diagonalization. This expansion is a natural choice for the NMR experiment where the tuned circuit of the NMR probe excites and detects in a band of frequencies associated with some definite Δm_I value. When implemented numerically this approach eliminates the need for high sampling rates and significantly decreases computation times. Additionally, this approach provides a general procedure for focusing on the excitation and detection of both fundamental, i.e., "Zeeman allowed" and overtone transitions.[21]

In the next section we outline our theoretical approach for treating excitation, detection, and sample rotation when the Zeeman eigenstates are not the system eigenstates. In a later section we present two illustrative examples when such a theoretical approach is necessary. These are (1) ^{14}N overtone NMR, where sensitivity issues associated with excitation bandwidth, detection, and sample rotation are more fully explored, and (2) third-order effects on nonsymmetric transitions, exploring examples of MAS, DOR, and ST-MAS spectra of half-integer and rotor synchronous acquisition MAS spectra of integer spin quadrupolar nuclei.

II. THEORY

To begin our treatment we define the laboratory frame by orienting the direction of the z axis along the static external magnetic field. We also define x-z plane to contain the axis of the excitation coil, where the excitation Hamiltonian in the laboratory frame is given by

$$\mathbf{H}_{\mathrm{rf}}(t)/\hbar = -2\gamma B_1 \cos(|\omega_{\mathrm{SF}}|t + \psi_{\mathrm{rf}})(\mathbf{I}_X \sin\chi_{\mathrm{rf}} + \mathbf{I}_Z \cos\chi_{\mathrm{rf}}). \quad (1)$$

Here γ is the gyromagnetic ratio of the nucleus being excited, B_1 is the excitation magnetic field strength, $|\omega_{\mathrm{SF}}|$ is the excitation frequency (i.e., spectrometer transmitter frequency), ψ_{rf} is the initial phase of the excitation, and χ_{rf} is the angle between the z-axis and the axis of the excitation coil. Likewise, the rf receiver coil is defined to have its axis in the x-z plane, and the signal detected by the receiver coil is given by

$$S_{\mathrm{coil}}(t) = \frac{d}{dt}\mathrm{Tr}\{\rho(t)\mathbf{I}_X\}\sin\chi_R + \frac{d}{dt}\mathrm{Tr}\{\rho(t)\mathbf{I}_Z\}\cos\chi_R, \quad (2)$$

where χ_R is the angle between the z-axis and the axis of the receiver coil.

In the absence of excitation the spins evolve under the stationary state Hamiltonian $\mathbf{H}_S$, whose representation in its diagonal frame $\mathbf{D}_S$ is related to the laboratory frame representation by

$$\mathbf{D}_S = \mathbf{V}^\dagger \mathbf{H}_S \mathbf{V}, \quad (3)$$

where $\mathbf{V}$ is a unitary transformation between the diagonal and laboratory frames. We will first consider a Hamiltonian whose diagonalization transformation, i.e., $\mathbf{V}$, is time independent. Later, we will consider the need for a time dependent diagonalization in the context of rotating samples and treat this problem using the adiabatic approximation.

If the Zeeman interaction is the dominant interaction in $\mathbf{H}_S$,

$$\mathbf{H}_S = \hbar\omega_0 \mathbf{I}_Z + \mathbf{H}_S^{(1)}, \quad (4)$$

where $\omega_0 = -\gamma B_0$ and $\mathbf{H}_S^{(1)}$ is the part of the stationary state Hamiltonian arising from spin couplings internal to the sample, then our treatment can be further simplified by moving into the "rotating tilted" frame,[20] a frame rotating about the z-axis of the diagonal frame, and defined by the following transformation:

$$\mathbf{W}(t) = \mathbf{V} e^{-i(\omega_{\mathrm{rot}}t + \phi_{\mathrm{rot}})\mathbf{I}_Z^\circ}, \quad (5)$$

where ω_{rot} is the rotating frame frequency and ϕ_{rot} is the initial phase of the rotating frame. All operators in this frame will carry a circle superscript. The orientation of the rotating tilted frame with respect to the laboratory frame will depend on crystallite orientation. The propagator in this frame is given by

$$\mathbf{U}^\circ(t,0) = \mathbf{T} e^{-(i/\hbar)\int_0^t [\mathbf{W}^\dagger(s)\mathbf{H}_S\mathbf{W}(s) + i\hbar\dot{\mathbf{W}}^\dagger(s)\mathbf{W}(s)]ds}, \quad (6)$$

where $\mathbf{T}$ is the time ordering operator, $\mathbf{W}^\dagger(t)\mathbf{H}_S\mathbf{W}(t)$ is the diagonalized laboratory frame stationary state Hamiltonian, and $i\hbar\dot{\mathbf{W}}^\dagger(t)\mathbf{W}(t)$ is the familiar quantum analogue of the inertial forces generated classically by transforming to a moving frame. This propagator can be related back to the lab frame according to

$$\mathbf{U}(t,0) = \mathbf{W}(t)\mathbf{U}^\circ(t,0)\mathbf{W}^\dagger(0). \quad (7)$$

The density operator in the rotating tilted frame $\rho^\circ(t)$ is related to the laboratory frame density operator by

$$\rho^\circ(t) = \mathbf{W}(t)^\dagger \rho(t) \mathbf{W}(t). \quad (8)$$

We follow the NMR experiment (i.e., define our coherences) in the rotating tilted frame.[22] Additionally, we take the equilibrium density operator in the high temperature approximation to be proportional to the stationary state Hamiltonian, that is,

$$\rho_{\mathrm{eq}}^\circ \propto \mathbf{D}_S. \quad (9)$$

In the treatment that follows we assume the Zeeman interaction is the dominant interaction in $\mathbf{H}_S$, and with the proper choice of ω_{rot} obtain a time independent "rotating tilted frame" Hamiltonian $\mathbf{H}^\circ$ in the form of

$$\mathbf{H}^\circ = \mathbf{W}(t)^\dagger \mathbf{H}_S \mathbf{W}(t) - \hbar\omega_{\mathrm{rot}}\mathbf{I}_Z^\circ + \mathbf{H}^\circ{}_{\mathrm{rf}}(n), \quad (10)$$

where $\mathbf{H}_{\mathrm{rf}}^\circ(n)$ is the effective rf Hamiltonian that excites the nth harmonic, that is, $n=1$ for the fundamental, $n=2$ for the first overtone, and so on. In this derivation we will also define $\Delta\omega = \omega_0 - \omega_{\mathrm{rot}}$, and assume that ω_{rot} is chosen so that $|\Delta\omega| \ll |\omega_0|$. Additionally, we adopt and modify the conven-

tion of Levitt,[23] and, depending on the sign of the gyromagnetic ratio and the harmonic to be excited or detected, further define

$$\phi_{\mathrm{rot}} = \begin{cases} 0 & \text{when } \gamma < 0, \\ \pi/n & \text{when } \gamma > 0. \end{cases} \tag{11}$$

To include rf excitation we assume that the magnitude of the excitation Hamiltonian is small compared to the stationary state Hamiltonian, i.e., $\|\mathbf{H}_S\| \gg \|\mathbf{H}_{\mathrm{rf}}(t)\|$ at all times. In this case the static diagonalization of $\mathbf{H}_S$ is used to transform the operators in the excitation Hamiltonian in Eq. (1) into the rotating tilted frame. The same approach will be applied to Eq. (2), our expression for the signal. Thus, to begin the derivation we transform the operators that appear in Eqs. (1) and (2) into the rotating tilted frame,

$$\mathbf{W}^{\dagger}(t)\mathbf{I}_X\mathbf{W}(t) = \sum_{l,m} X_{l,m}\mathcal{T}^{\circ}_{l,m}e^{-im(\omega_{\mathrm{rot}}t+\phi_{\mathrm{rot}})}, \tag{12}$$

and

$$\mathbf{W}^{\dagger}(t)\mathbf{I}_Z\mathbf{W}(t) = \sum_{l,m} Z_{l,m}\mathcal{T}^{\circ}_{l,m}e^{-im(\omega_{\mathrm{rot}}t+\phi_{\mathrm{rot}})}, \tag{13}$$

where

$$\begin{aligned} X_{l,m} &= \mathrm{Tr}(\mathbf{V}^{\dagger}\mathbf{I}_X\mathbf{V}\mathcal{T}^{\dagger}_{l,m}), \\ Z_{l,m} &= \mathrm{Tr}(\mathbf{V}^{\dagger}\mathbf{I}_Z\mathbf{V}\mathcal{T}^{\dagger}_{l,m}). \end{aligned} \tag{14}$$

For a spin I the integer values of l will run from 0 to $2I$, and m will cover integer values from $-l$ to l. Here, the $\mathcal{T}_{l,m}$ are the unit irreducible tensor operators, which satisfy the following trace relation:

$$\mathrm{Tr}\{\mathcal{T}_{l,m}\mathcal{T}^{\dagger}_{l',m'}\} = \delta_{l,l'}\delta_{m,m'}. \tag{15}$$

It is important not to confuse these operators with the nonunit irreducible tensor operators, which are more commonly used in theoretical descriptions of NMR Hamiltonians. The relationship between the unit $\mathcal{T}_{l,m}$ and nonunit $\mathbf{T}_{l,m}$ tensor operators is given by[24]

$$\mathcal{T}_{l,m} = \frac{1}{l!}\left[\frac{(2l+1)(2I-l)!2^l(2l)!}{((2I+l+1))!}\right]^{1/2}\mathbf{T}_{l,m}. \tag{16}$$

Equations (12)–(14) are key to developing our theoretical approach, and facilitate the analytical filtering needed in this problem.[22] In the sections that follow we will find it convenient to define

$$C_{l,m} = X_{l,m}\sin\chi_R + Z_{l,m}\cos\chi_R. \tag{17}$$

Using the static perturbation approach as outlined by Goldman *et al.*,[20] $\mathbf{V}$ can written in terms of a series expansion,

$$\mathbf{V} = 1 + \mathbf{V}^{(1)} + \mathbf{V}^{(2)} + \cdots, \tag{18}$$

with each correction expanded in terms of irreducible tensor operators. These expressions can then be substituted into Eq. (14) to obtain a perturbation expansion for $C_{l,m}$ (see Appendix B). Alternatively, one can employ numerical methods, where $\mathbf{V}$ (and $\mathbf{D}$) are calculated exactly and used in Eq. (14) to obtain an exact evaluation for $C_{l,m}$. In a numerical approach the returned eigenstates will likely be in the following form:

$$\mathbf{V}' = \mathbf{V}e^{-i\boldsymbol{\Xi}}, \tag{19}$$

where $[\boldsymbol{\Xi},\mathbf{D}]=0$. Thus, it is necessary to adjust the phase of each eigenvector column so the diagonal elements of $\mathbf{V}$ are real, as they are in Eq. (18). That is, the arbitrary phases from $\boldsymbol{\Xi}$ are simply removed. This ensures a proper evaluation of $X_{l,m}$ in Eq. (14).

A. Detection

Using Eqs. (12) and (13) with the detected signal given from Eq. (2) we find

$$S_{\mathrm{coil}}(t) = \sum_{l,m}\frac{d}{dt}C_{l,m}\mathrm{Tr}\{\rho^{\circ}(t)\mathcal{T}^{\circ}_{l,m}\}e^{-im(\omega_{\mathrm{rot}}t+\phi_{\mathrm{rot}})}. \tag{20}$$

Although intriguing, we will not consider further the weaker signal arising from the derivative of slow ($\ll\omega_{\mathrm{rot}}$) time dependence inside the $\mathrm{Tr}\{\rho^{\circ}(t)\mathcal{T}^{\circ}_{l,m}\}$ term in addition to the $m=0$ term. Since NMR probe bandwidths rarely extend over integer multiples of ω_{rot}, we select only signal from specific $\pm m$ values, that is, from the harmonic $n=|m|$. Under these conditions, we can expand Eq. (20) in terms of specific harmonic values, again adopting the modified phase convention of Levitt, to obtain

$$S_{\mathrm{coil}}(t) = -in\omega_{\mathrm{rot}}\frac{\gamma}{|\gamma|}\sum_{l=n}^{2I}[\Upsilon_{l,-n}(t)e^{in\omega_{\mathrm{rot}}t} - \Upsilon_{l,n}(t)e^{-in\omega_{\mathrm{rot}}t}], \tag{21}$$

where

$$\Upsilon_{l,n}(t) = C_{l,n}\,\mathrm{Tr}\{\rho^{\circ}(t)\mathcal{T}^{\circ}_{l,n}\}. \tag{22}$$

Within the NMR spectrometer this signal is mixed down with a receiver reference oscillation $|\omega_{\mathrm{SF}}|$ to lower frequencies where it can be more easily recorded. Mathematically, this mixing process is simulated by multiplying the signal detected in the receiver coil by $2\cos(|\omega_{\mathrm{SF}}|t+\psi_{\mathrm{ref}})$, to obtain

$$S_{\cos}(t) = 2\cos(|\omega_{\mathrm{SF}}|t+\psi_{\mathrm{ref}})S_{\mathrm{coil}}(t), \tag{23}$$

and by $2\sin(|\omega_{\mathrm{SF}}\,t+\psi_{\mathrm{ref}})$ to obtain

$$S_{\sin}(t) = 2\sin(|\omega_{\mathrm{SF}}|t+\psi_{\mathrm{ref}})S_{\mathrm{coil}}(t). \tag{24}$$

We define the phase of the reference as $\psi_{\mathrm{ref}}=-(\gamma/|\gamma|)\phi_R$. Depending on the receiver frequency $|\omega_{\mathrm{SF}}|$ and the sign of the gyromagnetic ratio we eliminate all terms that contain frequencies that are outside the detection bandwidth of the NMR probe. This is a good approximation, since NMR probe bandwidths are typically too small to detect over a range that is integer mulitples of ω_0. Thus, we neglect the fast $n\omega_{\mathrm{rot}}+|\omega_{\mathrm{SF}}|$ oscillations for positive Larmor frequencies, i.e., $\gamma<0$, or the fast $n\omega_{\mathrm{rot}}-|\omega_{\mathrm{SF}}|$ oscillations for negative Larmor frequencies, i.e., $\gamma>0$. In the experiment we will set the receiver frequency to match selected integer multiples of the rotating frame frequency so that

$$n\omega_{\mathrm{rot}} + \frac{\gamma}{|\gamma|}|\omega_{\mathrm{SF}}| = \begin{cases} n\omega_{\mathrm{rot}} - |\omega_{\mathrm{SF}}| = 0 & \text{when } \gamma < 0, \\ n\omega_{\mathrm{rot}} + |\omega_{\mathrm{SF}}| = 0 & \text{when } \gamma > 0. \end{cases} \tag{25}$$

From this we obtain $\omega_{\mathrm{rot}} = -(\gamma/|\gamma|)|\omega_{\mathrm{SF}}|/n$ and simplify our two signal expressions to

$$S_{\cos}(n,t) = i|\omega_{\mathrm{SF}}| \sum_{l=n}^{2I} [\Upsilon_{l,-n}(t)e^{-i\phi_R} - \Upsilon_{l,n}(t)e^{i\phi_R}], \tag{26}$$

and

$$S_{\sin}(n,t) = \frac{\gamma}{|\gamma|}|\omega_{\mathrm{SF}}| \sum_{l=n}^{2I} [\Upsilon_{l,-n}(t)e^{-i\phi_R} + \Upsilon_{l,n}(t)e^{i\phi_R}]. \tag{27}$$

Depending on the sign of the gyromagnetic ratio we combine these two real signals in the spectrometer into a complex signal given by

$$S(n,t) = S_{\cos}(n,t) - i(\gamma/|\gamma|)S_{\sin}(n,t), \tag{28}$$

which leads to our final expression for the NMR signal as follows:

$$S(n>0,t) = -i2|\omega_{\mathrm{SF}}| \sum_{l=n}^{2I} C_{l,n} \operatorname{Tr}\{\rho^{\circ}(t)\mathcal{T}^{\circ}_{l,n}\}e^{i\phi_R}. \tag{29}$$

This expression highlights a number of important features of the signal when strong quadrupolar couplings are present. First, we examine a zeroth-order approximation for the eigenstates where one finds (see Appendix B) that $C_{1,1}$, given by

$$C_{1,1} = -\frac{1}{\sqrt{2}} f_I^{(0)} \sin \chi_R, \tag{30}$$

where

$$f_I^{(0)} = \left[\frac{I(I+1)(2I+1)}{3} \right]^{1/2}, \tag{31}$$

is the only nonzero coefficient. As expected, the resulting fundamental signal,

$$S(n=1,t) = i|\omega_{\mathrm{SF}}|\sqrt{2} f_I^{(0)} \operatorname{Tr}\{\rho^{\circ}(t)\mathcal{T}^{\circ}_{1,1}\}e^{i\phi_R} \sin \chi_R, \tag{32}$$

varies in strength as the sine of the angle between the axis of the coil and B_0, becoming unobservable when the coil is parallel to B_0. Additionally, combining the use of a Faraday detection scheme, which is linearly dependent on detection frequency, with an equilibrium magnetization, which is linearly dependent on ω_0 in the high temperature approximation, we also find the expected behavior that the overall fundamental signal strength increases with ω_0^2.[25]

With a first-order correction to the eigenstates the direct detection of the first overtone ($n=2$) signal becomes possible. In the case of a strong quadrupolar coupling, where we write the full quadrupolar Hamiltonian[40] in the laboratory frame as

$$\mathbf{H}_q = \hbar\omega_q \sum_{k=-2}^{2} (-1)^k A_{2,k} \mathbf{T}_{2,-k}, \tag{33}$$

with the quadrupolar splitting given by

$$\omega_q = 6\pi C_q / 2I(2I-1), \tag{34}$$

with C_q as the quadrupolar coupling constant, the $n=2$ overtone signal expression using a first-order eigenstate expansion of the $C_{l,n}$ for a spin $I=1$ nucleus gives

$$S(n=2,t) = -i2|\omega_{\mathrm{SF}}| \frac{\omega_q}{\omega_0} f_I^{(0)} f_I^{(1)} \operatorname{Tr}\{\rho^{\circ}(t)\mathcal{T}^{\circ}_{2,2}\} \times [A_{2,-2}(\Omega_q)\cos\chi_R - A_{2,-1}(\Omega_q)\sin\chi_R]e^{i\phi_R}, \tag{35}$$

where

$$f_I^{(1)} = \frac{1}{\sqrt{120}} \left[\frac{(2I+3)!}{(2I-2)!} \right]^{1/2}. \tag{36}$$

Here, we see the well known result that overtone signals can be detected at nearly equal strength with the axis of the coil at any angle with respect to B_0, including parallel. Notice that the inverse dependence on the static field strength cancels part of the sensitivity advantages of high frequency detection, that is, ω_0 cancels $|\omega_{\mathrm{SF}}|$ and one finds that the first overtone signal strength only increases linearly with ω_0. This effect was predicted by Tycko and Opella.[21] With each successive higher-order eigenstate correction, the next higher harmonic signal becomes allowed, up to the maximum allowed harmonic of $n=2I$. Using this approach, one can readily show that the nth harmonic signal strength will vary according to $\omega_0^2(\omega_q/\omega_0)^{n-1}$. Interestingly, with higher-order eigenstate corrections the fundamental ($n=1$) signal also contains "Zeeman" forbidden contributions from the $l>1$ terms. These contributions, however, are scaled by the $C_{l,n}$, whose magnitude decreases as $(\omega_q/\omega_0)^{l-1}$. Normally, such signal contributions are not detected as the contribution from the lowest value of l will always dominant.

For overtone signals, there is a strong crystallite orientation dependence inside the $C_{l,n}$ term. This complex scaling will lead to each crystallite having its own unique signal phase and amplitude. From this one might conclude that there would be no observable coherence, since the net signal from all the crystallites with such a distribution of effective receiver phases would be zero. However, as explained by Marinelli *et al.*,[26] an identical crystallite dependent phase shift is present in the phase of the excitation pulse. Thus, the magnetization vectors after a pulse are distributed in such a way that the signal from these "dephased" magnetization vectors are reassembled into a coherent signal. If, however, the crystallite orientation changes between excitation and detection, as would occur with sample rotation, then a complex spinning sideband pattern and a dramatic loss of signal occurs.[26] This behavior is illustrated in Sec. IV.

B. Excitation

Inserting Eqs. (12) and (13) into the excitation Hamiltonian and again using the modified Levitt convention to obtain an excitation Hamiltonian that is independent of the sign of the gyromagnetic ratio, we define $\omega_1 = |\gamma B_1|$ and $\psi_{\mathrm{rf}} = -(\gamma/|\gamma|)\phi$ to obtain

$$\mathbf{H}^{\circ}_{\mathrm{rf}}(t)/\hbar = 2\omega_1 \cos\left(|\omega_{\mathrm{SF}}|t - \frac{\gamma}{|\gamma|}\phi\right)\sum_{l,m} C_{l,m}\mathcal{T}^{\circ}_{l,m}e^{-im\omega_{\mathrm{rot}}t}. \tag{37}$$

Neglecting the possibility of excitation through the $m=0$ term, and expanding in terms of transition harmonic values, n, we obtain

$$\begin{aligned}\mathbf{H}^{\circ}_{\mathrm{rf}}(t)/\hbar\omega_1 = &\sum_{l,n>0} C_{l,n}\mathcal{T}^{\circ}_{l,n}[e^{-i(n\omega_{\mathrm{rot}}-|\omega_{\mathrm{SF}}|)t}e^{-i(\gamma/|\gamma|)\phi} \\ &+ e^{-i(n\omega_{\mathrm{rot}}+|\omega_{\mathrm{SF}}|)t}e^{i(\gamma/|\gamma|)\phi}] \\ &+ \sum_{l,n>0} C_{l,-n}\mathcal{T}^{\circ}_{l,-n}[e^{i(n\omega_{\mathrm{rot}}-|\omega_{\mathrm{SF}}|)t}e^{i(\gamma/|\gamma|)\phi} \\ &+ e^{i(n\omega_{\mathrm{rot}}+|\omega_{\mathrm{SF}}|)t}e^{-i(\gamma/|\gamma|)\phi}].\end{aligned} \tag{38}$$

Depending on the transmitter frequency $|\omega_{\mathrm{SF}}|$ and the sign of the gyromagnetic ratio we eliminate all terms in the above expression that contain frequencies that are outside the excitation bandwidth of the NMR probe. Again, this is a good approximation, since NMR probe bandwidths are typically too small to excite over a range that spans integer mulitples of ω_0. Thus, we neglect the fast $n\omega_{\mathrm{rot}}+|\omega_{\mathrm{SF}}|$ oscillations for a positive Larmor frequencies, i.e., $\gamma<0$, or the fast $n\omega_{\mathrm{rot}}-|\omega_{\mathrm{SF}}|$ oscillations for a negative Larmor frequencies, i.e., $\gamma>0$. As before, we will not consider here excitation associated with $n=0$, that is, dc pulses. We set the transmitter frequency to match selected integer multiple of the rotating frame frequency according to Eq. (25), again implying a rotating frame frequency given by $\omega_{\mathrm{rot}}=-(\gamma/|\gamma|)|\omega_{\mathrm{SF}}|/n$. Under these conditions we obtain the excitation Hamiltonian

$$\mathbf{H}^{\circ}_{\mathrm{rf}}(n>0) = \hbar\omega_1\sum_{l=n}^{2I}[C_{l,n}\mathcal{T}^{\circ}_{l,n}e^{i\phi} + C_{l,-n}\mathcal{T}^{\circ}_{l,-n}e^{-i\phi}]. \tag{39}$$

As with the signal, we can apply a zeroth-order approximation for the eigenstates, and find the fundamental rf excitation Hamiltonian,

$$\mathbf{H}^{\circ}_{\mathrm{rf}}(n=1) = -\hbar\omega_1\frac{f^{(0)}_I}{\sqrt{2}}[\mathcal{T}^{\circ}_{1,1}e^{i\phi} - \mathcal{T}^{\circ}_{1,-1}e^{-i\phi}]\sin\chi_{\mathrm{rf}}. \tag{40}$$

Again, note that the fundamental rf excitation strength varies as the sine of angle between the axis of the coil and B_0, with no excitation possible when the coil is parallel to B_0. With a first-order correction to the eigenstates the direct excitation of the first overtone, i.e., $n=2$, signal becomes possible. In the case of a strong quadrupolar coupling in a spin $I=1$ nucleus, the $n=2$ overtone excitation is given by

$$\begin{aligned}\mathbf{H}^{\circ}_{\mathrm{rf}}(n=2) = &\frac{\hbar\omega_1\omega_q}{\omega_0}f^{(0)}_I f^{(1)}_I[\mathcal{T}^{\circ}_{2,2}[A_{2,-2}(\Omega_q)\cos\chi_{\mathrm{rf}} \\ &- A_{2,-1}(\Omega_q)\sin\chi_{\mathrm{rf}}]e^{i\phi} + \mathcal{T}^{\circ}_{2,-2}[A_{2,2}(\Omega_q)\cos\chi_{\mathrm{rf}} \\ &+ A_{2,1}(\Omega_q)\sin\chi_{\mathrm{rf}}]e^{-i\phi}].\end{aligned} \tag{41}$$

As before, the complex scaling from the $C_{l,n}$ coefficients lead to each crystallite having its own unique transmitter phase and strength during overtone excitation. It is the matching of this phase to the "effective" overtone receiver phase of each crystallite that leads to a net observable overtone signal in polycrystalline samples. Additionally, with each successive higher-order eigenstate correction, the excitation of higher overtone signals become possible, with n values up to $2I$. Again, note that with higher-order eigenstate corrections it becomes possible to excite fundamental $(n=1)$ transitions through "Zeeman" forbidden contributions in the $l>1$ terms. Finally, we point out that while most phase cycling relationships for coherence transfer pathways will be unaffected by higher-order effects, there are some situations that may require a modified approach, particularly, for coherence transfer between excitations associated with different harmonics n values.[22]

1. Off-resonant excitation

In our treatment above, we have chosen to use a common rotating frame where both excitation and detection occurs. This is somewhat restrictive, since it is often necessary to apply excitation pulses at multiple frequencies during an experiment. It is still useful to define a common rotating frame particularly, since signals are often detected inside the common rotating frame. Thus, when treating off-resonant excitation, we will define offset rotating frames with respect to our common rotating frame. When applying excitation at a frequency offset $\Delta\omega$ from $|\omega_{\mathrm{SF}}|$, one transforms into an offset rotating frame, given by

$$\omega'_{\mathrm{rot}} = -\frac{\gamma}{|\gamma|}|\omega_{\mathrm{SF}} + \Delta\omega|/n. \tag{42}$$

In this frame the Hamiltonian of Eq. (39) is used to construct the offset rotating frame Hamiltonian, given by

$$\mathbf{H}'^{\circ} = \mathbf{W}(t)^{\dagger}\mathbf{H}_S\mathbf{W}(t) - \hbar\omega'_{\mathrm{rot}}\mathbf{I}^{\circ}_Z + \mathbf{H}^{\circ}_{\mathrm{rf}}(n). \tag{43}$$

This Hamiltonian can then be used to construct the propagator in the common rotating frame according to

$$\mathbf{U}^{\circ}(t_b,t_a) = e^{-i\Delta\omega_{\mathrm{rot}}t_b\mathbf{I}^{\circ}_Z}e^{-(i/\hbar)\mathbf{H}'^{\circ}(t_b-t_a)}e^{i\Delta\omega_{\mathrm{rot}}t_a\mathbf{I}^{\circ}_Z}, \tag{44}$$

where $\Delta\omega_{\mathrm{rot}}=\omega'_{\mathrm{rot}}-\omega_{\mathrm{rot}}$.

C. Rotating samples

Through sample motion the orientation of the principal axis system for the internal spin interactions with respect to the laboratory frame becomes time dependent. For systems with second- and higher-order effects this introduces a complication that the direction of the eigenstates in the laboratory frame is time dependent. Fortunately, this situation can be simplified in solid-state NMR since the time dependence from sample motion is slow enough that we can make the adiabatic approximation. In making this approximation, however, care must be taken to properly correct for any quantum mechanical anholonomy. That is, time-dependent eigenstates do not return to their original values after completing a cyclic evolution period, but rather acquire an additional phase modulation that depends on the geometry of the path traversed by the eigenstates during sample motion.

To treat this situation we will transform into a rotating frame about the z-axis of the diagonal frame (i.e., the rotating tilted frame), using

$$\mathbf{W}(t) = \mathbf{V}(t)e^{-i\Gamma(t)}\mathbf{Z}(t), \tag{45}$$

where

$$\mathbf{Z}(t) = e^{-i(\omega_{\text{rot}}t+\phi_{\text{rot}})\mathbf{I}_Z^\circ}, \tag{46}$$

and $\Gamma(t)$ will be defined below. We write the propagator as

$$\mathbf{U}(t) = \mathbf{W}(t)\mathbf{T}e^{-(i/\hbar)\int_0^t[\mathbf{D}(\mathbf{s})+i\hbar\dot{\mathbf{W}}^\dagger(s)\mathbf{W}(s)]ds}\mathbf{W}^\dagger(0), \tag{47}$$

where

$$i\dot{\mathbf{W}}^\dagger(t)\mathbf{W}(t) = \mathbf{Z}^\dagger(t)[e^{i\Gamma(t)}\dot{\mathbf{V}}^\dagger(t)\mathbf{V}(t)e^{-i\Gamma(t)} - \dot{\Gamma}(t)]\mathbf{Z}(t) - \omega_{\text{rot}}\mathbf{I}_Z^\circ.$$

We make the adiabatic approximation by neglecting all the parts of $i\dot{\mathbf{V}}^\dagger(t)\mathbf{V}(t)$ that do not commute with $\mathbf{D}(t)$. Furthermore, one can show that enforcing parallel transport of the time dependent eigenstates $|n(t)\rangle$, using the constraint

$$\langle n(t)|\dot{n}(t)\rangle = 0, \tag{48}$$

leads to

$$\langle n(t)|e^{i\Gamma(t)}i\dot{\mathbf{V}}^\dagger(t)\mathbf{V}(t)e^{-i\Gamma(t)} - \dot{\Gamma}(t)|n(t)\rangle = 0. \tag{49}$$

Thus, we enforce parallel transport of the eigenvectors by defining

$$\dot{\Gamma}(t) = i\sum_n |\dot{n}(t)\rangle\langle n(t)| = i[\dot{\mathbf{V}}^\dagger(t)\mathbf{V}(t)]_{\text{diag}}. \tag{50}$$

In the adiabatic limit the propagator in the rotating tilted frame becomes

$$\mathbf{U}^\circ(t,0) = e^{-i\int_0^t\dot{\mathbf{\Gamma}}(s)ds}e^{-(i/\hbar)\int_0^t[\mathbf{D}(s)-\hbar\omega_{\text{rot}}\mathbf{I}_Z^\circ]ds}. \tag{51}$$

In the case of a strong quadrupolar coupling, one can show,[20] using a first-order correction to the eigenstates, that $\dot{\mathbf{\Gamma}}(t)$ is given by

$$\dot{\mathbf{\Gamma}}^{(1)}(t) = -\frac{i}{2}\left(\frac{\omega_Q}{\omega_Z}\right)^2\sum_{m\neq 0}\frac{\dot{A}_{2m}(t)A_{2-m}(t)[\mathbf{T}_{2-m},\mathbf{T}_{2m}]}{m^2}. \tag{52}$$

Since the magnitude of the excitation Hamiltonian is small compared to $\mathbf{D}(t)$, it can be added without affecting the time dependent tilting of $\mathbf{V}(t)$. Thus, with the proper choice of ω_{rot}, we obtain an effective Hamiltonian in the rotating tilted frame,

$$\mathbf{H}^\circ(t) = \mathbf{D}(t) - \hbar\omega_{\text{rot}}\mathbf{I}_Z^\circ + \dot{\mathbf{\Gamma}}(t) + \mathbf{H}_{\text{rf}}^\circ(t,n), \tag{53}$$

where the excitation Hamiltonian is given by

$$\mathbf{H}_{\text{rf}}^\circ(n>0) = \hbar\omega_1\sum_{l=n}^{2I}[C_{l,n}(t)\mathcal{T}_{l,n}^\circ e^{i\phi} + C_{l,-n}(t)\mathcal{T}_{l,-n}^\circ e^{-i\phi}]. \tag{54}$$

Equations (12), (13), and (17) can still be used with the time dependent $\mathbf{V}(t)$ to obtain time dependent coefficients $C_{l,m}(t)$. The signal is then given by

$$S(n>0,t) = -i2|\omega_{\text{SF}}|\sum_{l=n}^{2I}C_{l,n}(t)\ \text{Tr}\{\rho^\circ(t)\mathcal{T}_{l,n}^\circ\}e^{i\phi_R}. \tag{55}$$

III. NUMERICAL METHODS

To treat a time dependent Hamiltonian in numerical calculations we adopt the conventional approach of dividing time into small enough dt values that the Hamiltonian can be approximated as time independent. For the evolution of the density operator in the laboratory frame we construct the propagator according to

$$\mathbf{U}(ndt,0) = \mathbf{U}_n\cdots\mathbf{U}_1\mathbf{U}_0, \tag{56}$$

where

$$\mathbf{U}_n = \mathbf{V}_n e^{-(i/\hbar)\mathbf{D}_n dt}\mathbf{V}_n^\dagger. \tag{57}$$

We prefer, however, to evolve the density operator in the rotating tilted frame where it is easier to separate resonances according to harmonics. The numerical transformation of the density operator into the initial tilted frame is

$$\rho_0^\circ = \mathbf{W}_0^\dagger\rho_0\mathbf{W}_0, \tag{58}$$

where we define the following transformation:

$$\mathbf{W}_n = \mathbf{V}_n\mathbf{Z}_n, \tag{59}$$

and

$$\mathbf{Z}_n = e^{-i(\omega_{\text{rot}}ndt\mathbf{I}_Z^\circ+\phi_{\text{rot}})}. \tag{60}$$

Similarly, we can relate the laboratory frame propagators $\mathbf{U}_n$ to the tilted rotating frame propagators $\mathbf{U}_n^\circ$ according to

$$\mathbf{U}^\circ(ndt,0) = \underbrace{\mathbf{W}_{n+1}^\dagger\mathbf{U}_n\mathbf{W}_n}_{\mathbf{U}_n^\circ}\cdots\underbrace{\mathbf{W}_2^\dagger\mathbf{U}_1\mathbf{W}_1}_{\mathbf{U}_1^\circ}\cdot\underbrace{\mathbf{W}_1^\dagger\mathbf{U}_0\mathbf{W}_0}_{\mathbf{U}_0^\circ}.$$

Combining Eqs. (57) and (59), we write the nth propagator in the tilted rotating frame as

$$\mathbf{U}_n^\circ = \mathbf{W}_{n+1}^\dagger\mathbf{U}_n\mathbf{W}_n = \mathbf{Z}_{n+1}^\dagger[\mathbf{V}_{n+1}^\dagger\mathbf{V}_n]e^{-(i/\hbar)\mathbf{D}_n dt}\mathbf{Z}_n. \tag{61}$$

In our numerical approach we apply the adiabatic approximation by replacing the expression in square brackets with

$$[\mathbf{V}_{n+1}^\dagger\mathbf{V}_n] \rightarrow e^{-i\dot{\mathbf{\Gamma}}_n dt}, \tag{62}$$

where

$$\dot{\mathbf{\Gamma}}_n dt = i[[\mathbf{V}_{n+1}^\dagger - \mathbf{V}_n^\dagger]\mathbf{V}_n]_{\text{diag}}. \tag{63}$$

One can show, using a series expansion of Eq. (62), that the adiabatic approximation can be further simplified to

$$[\mathbf{V}_{n+1}^\dagger\mathbf{V}_n] \rightarrow [\mathbf{V}_{n+1}^\dagger\mathbf{V}_n]_{\text{diag}}, \tag{64}$$

and the nth propagator becomes

$$\mathbf{U}_n^\circ = [\mathbf{V}_{n+1}^\dagger\mathbf{V}_n]_{\text{diag}}e^{-(i/\hbar)(\mathbf{D}_n-\hbar\omega_{\text{rot}}\mathbf{I}_Z^\circ)dt}. \tag{65}$$

All simulations were performed using 6044 crystal orientations from the three angle zcw set.[27–30]

IV. EXAMPLES

Using the theoretical approach outlined in this paper, we have performed full density operator numerical simulations of illustrative examples where higher-order effects are necessary to describe the experiment.

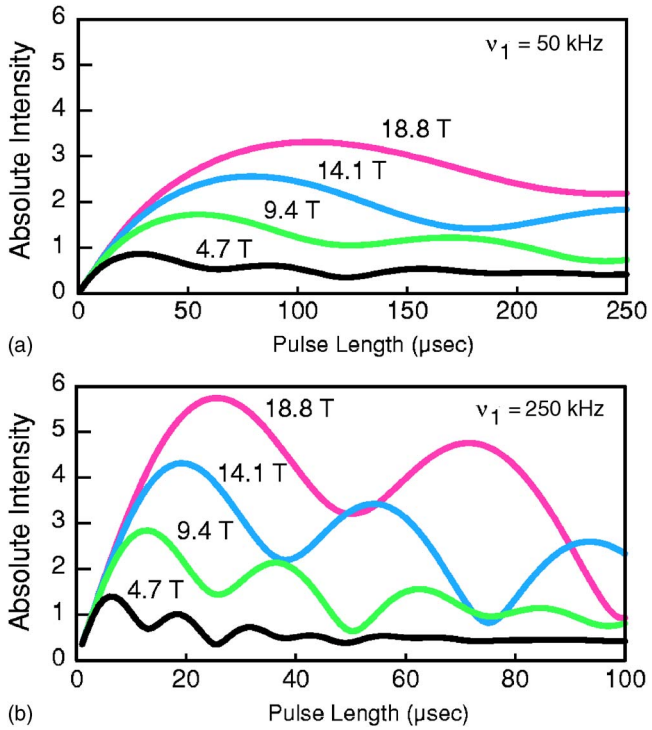

FIG. 1. (Color online) Comparison of absolute intensity of simulated ^{14}N static overtone of N-acetylvaline as a function of pulse length at 4.7, 9.4, 14.1, and 18.8 T with (a) ν_1=50 kHz and (b) ν_1=250 kHz. For both excitation and detection the coil was oriented at 90° with respect to B_0, that is, $\chi_{rf}=\chi_R=\pi/2$. Spectra were excited with the strongest singularity on resonance. N-acetylvaline ^{14}N parameters: δ_{csa}=106, η_{csa}=0.27, C_q=3.21 MHz, and η_q=0.31 with coincident tensor orientations assumed. Calculations were performed using exact eigenvalues and exact eigenvectors.

A. Nitrogen-14 overtone spectroscopy

The direct excitation and detection of overtone ($n>1$) transitions in solid-state NMR requires tilting of the eigenstates away from the Zeeman eigenstates. This possibility was experimentally demonstrated by Bloom and LeGros[31] and Tycko and Opella[21,32,33] with the ^{14}N overtone transition. While this transition is notoriously difficult to excite and detect it has an advantage over the fundamental transitions of ^{14}N that it does not experience first-order quadrupolar broadenings, and contributions from the second-order quadrupolar broadenings and remaining first-order interactions are typically on the order of a few kilohertz. Additionally, ^{14}N NMR does not required isotopic labeling. With the development of DOR and DAS, it was hoped that the remaining second-order anisotropy could be eliminated and high-resolution ^{14}N overtone spectra obtained. Alas, this possibility has proved elusive. In fact, even magic-angle spinning overtone experiments have been extremely difficult. The difficulty with sample rotation and overtone NMR was first explained by Marinelli *et al.*,[26] and we refer the reader there for additional details. Generally, overtone NMR is best understood by a close examination of the expressions for the excitation and signal after substituting the first-order expression for the $C_{l,n}$ (see Appendix B) into Eqs. (29) and (39). From Eq. (41) we see that the effective overtone nutation frequency has a $\omega_1\omega_q/\omega_0$ dependence as well as an orientation dependence. Figure 1 is a simulated comparison of absolute intensity of ^{14}N static overtone signal using the ^{14}N NMR parameters of N-acetylvaline as a function of pulse length at various static and rf field strengths. As predicted, the nutation frequency decreases with increasing static field strength, and there is a decay of the nutation oscillation due to the orientation dependence. Note that signal strengths at constant rf field strength increase linearly, as predicted, with increasing static field strength when using optimized pulse lengths.

Figures 2(a) and 2(b) are a comparison of simulated static overtone spectra for a ^{14}N site in N-acetylvaline at 4.7, 9.4, 14.1, and 18.8 T at two different radio frequency field strengths. As noted in earlier studies, ^{14}N overtone resonances are typically on the order of a few kilohertz, since their linewidths are dominated by second-order anisotropic broadenings from the quadrupolar interaction. The powder pattern lineshape, however, differs from the central transition lineshape of half-integer nuclei mainly from the strong dependence of excitation and detection on crystallite orienta-

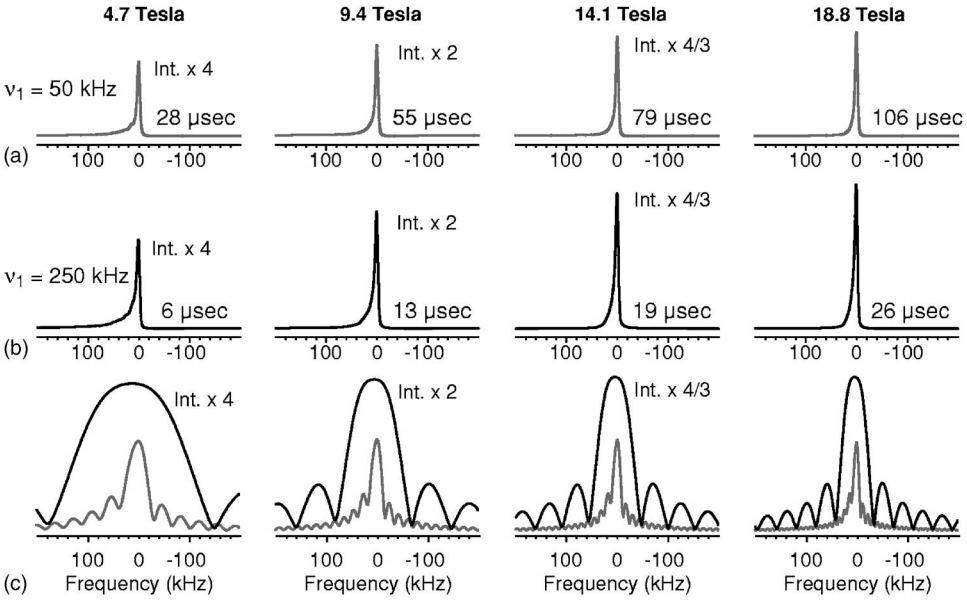

FIG. 2. Comparison of simulated ^{14}N static overtone spectrum of N-acetylvaline at 4.7, 9.4, 14.1, and 18.8 T with (a) ν_1=50 kHz and (b) ν_1=250 kHz. Spectra were excited with the strongest singularity on resonance, and pulses lengths optimized to values shown to obtain the maximum signal for each B_0 and B_1 field strength. (c) Offset dependence of ^{14}N static overtone excitation of N-acetylvaline at 4.7, 9.4, 14.1, and 18.8 T. Simulations with ν_1=50 kHz are shown in gray. For both excitation and detection the coil was oriented at 90° with respect to B_0, that is, $\chi_{rf}=\chi_R=\pi/2$. Calculations were performed using exact eigenvalues and exact eigenvectors.

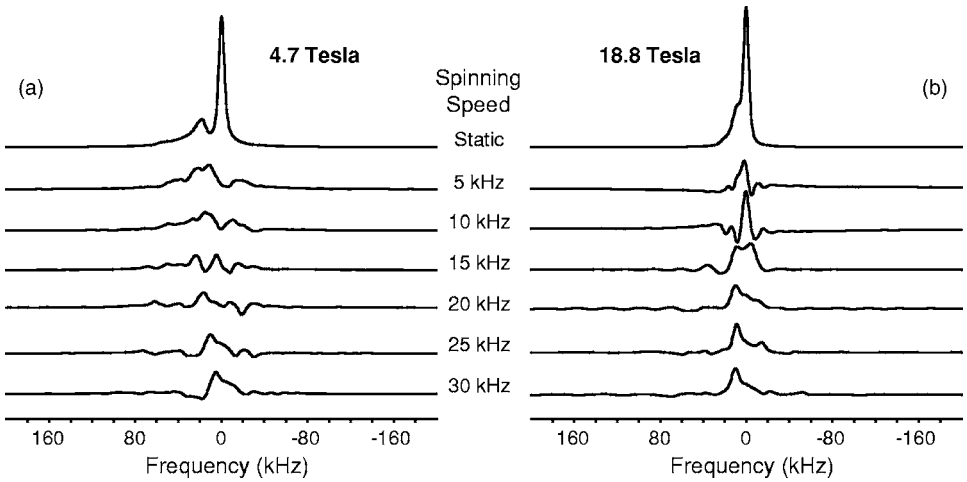

FIG. 3. Comparison of simulated ^{14}N static overtone magic-angle spinning spectra of N-acetylvaline at (a) 4.7 T and (b) 18.8 T with $\nu_1=50$ kHz. Spectra were excited with the strongest singularity on resonance, and pulse lengths of (a) 20 μs and (b) 100 μs, optimized on the static sample, was used in simulations. For both excitation and detection the coil was oriented at the magic-angle, that is, $\chi_{rf}=\chi_R=54.74°$. Calculations were performed using exact eigenvalues and eigenvectors. The intensity of the spectra in (a) were scaled by a factor of 4 compared to those in (b).

tion. One of the main experimental obstacles to overtone NMR, however, is the strong offset excitation dependence which arises from the orientation dependence and scaling of the rf field strength by ω_q/ω_0. This can be seen in Fig. 2(c). Only at the lowest static field and highest rf field strengths is the offset dependence somewhat reasonable. Clearly, it is difficult to excite and detect overtone resonances unless on-resonance excitation is applied. This has been a serious limitation of all overtone NMR experiments to date. Lee and Ramamoorthy[34] were able to reduce the offset dependence in ^{14}N overtone NMR somewhat with the use of composite pulses, however, the effect is rather severe and more significant improvements are clearly needed.

If the offset dependence were the only obstacle, overtone NMR could be developed into a more routine method. Unfortunately, when MAS is applied in overtone experiments the signal is nearly destroyed. This is demonstrated in Fig. 3 for the case of MAS at two different static field strengths. As noted earlier, as long as the orientation dependent phase of the rf excitation is identical to the orientation dependent phase of the detection there is constructive interference of signals from the different crystallites. With sample rotation, however, this phase matching is destroyed, and signals excited with one phase are detected with different phases as the sample rotates. The result is a significant loss in sensitivity, as illustrated in Fig. 3 for a polycrystalline sample. Additionally, as described by Marinelli *et al.*,[26] the time-dependent signal phase modulation due to sample motion splits the signal into a centerband and four spinning sidebands positioned at $0, \pm\Omega_R$, and $\pm 2\Omega_R$, respectively. With increasing spinning speeds the integrated intensity of the sidebands do not transfer to the centerband. This splitting occurs in addition to the normal spinning sidebands generated by rotational echoes of refocused frequency anisotropies.

Since the development of techniques for removing second-order anisotropies there has been excitement about the possibility of obtaining high resolution spectra from the ^{14}N overtone NMR transition, particularly, for the case of biomolecules. With the theoretical framework developed here we can properly investigate this possibility. Figure 4 is the simulated ^{14}N overtone double rotation spectra of N-acetylvaline at various spinning speeds and different static field strengths. As hoped, overtone DOR does eliminate second-order anisotropies. Unfortunately, overtone DOR suffers from the same limitations of MAS, that is, destructive interference of signals from the different crystallites occurs as the sample rotates, and the signal is split into many sidebands whose intensity do not transfer to the centerband with increased spinning speeds.

B. Nonsymmetric transitions

The symmetric $(m\rightarrow -m)$ transition of a quadrupolar nucleus is unaffected by the quadrupolar interaction to first-order in a perturbation expansion of the transition frequency. In fact, the symmetric transitions are also unaffected by the quadrupolar interaction to third-order in the perturbation expansion of their transition frequencies.[35] For this reason the central $(1/2\rightarrow -1/2)$ transition is the most easily excited and detected transition in solid-state NMR of half-integer quadrupolar nuclei in polycrystalline samples. In contrast, the

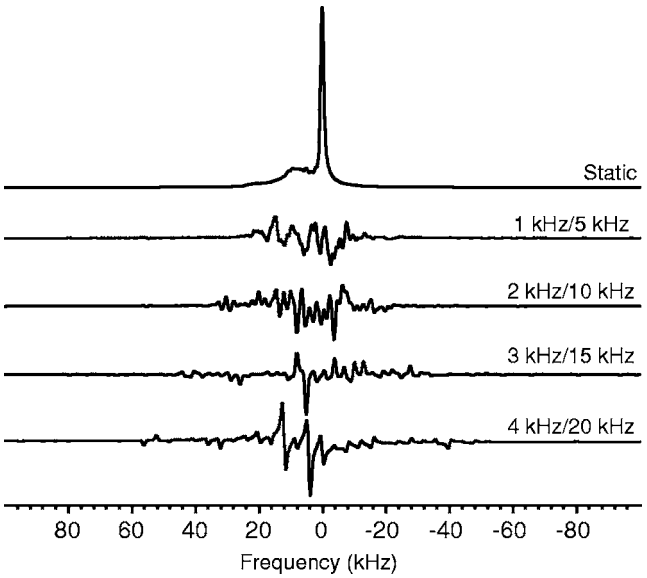

FIG. 4. Comparison of simulated ^{14}N overtone double rotation spectra of N-acetylvaline at 18.8 T with $\nu_1=50$ kHz. Inner/outer rotor spinning speeds are as indicated. Spectra were excited with the strongest singularity on resonance, and a pulse length of 100 μs, optimized on the static sample, was used in all simulations. For both excitation and detection the coil was oriented at the magic-angle, that is, $\chi_{rf}=\chi_R=54.74°$. Calculations were performed using exact eigenvalues and eigenvectors.

nonsymmetric transitions are affected by the quadrupolar interaction at all orders in the perturbation expansion of their transitions frequencies. Thus, in polycrystalline solids, the anisotropic linewidth of the satellite transitions are typically orders of magnitude larger than the symmetric transitions. Nonetheless, there are a number of advantages to exciting and detecting the nonsymmetric satellite transitions[36] for probing the structure as well as the dynamics[37] in materials. This has been particularly true after the introduction of the ST-MAS experiment,[6,38] which provides a high resolution spectrum through a two-dimensional correlation between the satellite and central transition. In the case of ^{27}Al NMR in Andalusite, however, the ST-MAS experiment is unable to produce an isotropic spectrum of the site with the largest quadrupolar couplings[8] at a magnetic field strength of 11.7 T. Using static perturbation theory, Gan *et al.*[8] obtained analytical expressions for the third-order energy eigenvalues and numerically simulated the ST-MAS spectrum. They found that the anisotropy arising from the third-order term is sizable, and destroys the mirror image symmetry needed between the central and the satellite transitions to refocus completely the anisotropy, which in turn spoils the ability of the ST-MAS experiment to provide a high-resolution isotropic dimension. Using our theoretical approach we have numerically simulated ST-MAS spectra (shown in Fig. 5), using the NMR parameters of the large C_q site in Andalusite. In the left column are ST-MAS spectra simulated using second-order eigenvalues with zeroth-order eigenstates. In the right column are ST-MAS spectra simulated using exact eigenvalues with zeroth-order eigenstates. This figure reproduces the result of Gan *et al.*[8] and additionally highlights the differences between the observed (exact) spectra and the spectra predicted using only second-order perturbation theory. At the top in both columns are the simulated ST-MAS spectra spinning at the magic-angle. Clearly, the third- and higher-order effects are responsible for the loss of the high resolution correlation. Moving down from the top in both columns are ST-MAS spectra obtained at angles slightly away from the magic angle. The ST-MAS experiment is notoriously sensitive to mis-set of the magic-angle, and these spectra show how the residual 2D lineshape arising from the third-order term could easily be misinterpreted as an angle mis-set, rather than a third-order effect.

To better understand this effect, we have simulated the static, MAS, DOR, and triple rotation (TIR) spectra of ^{27}Al NMR in Andalusite. While third-order effects are difficult to discern in the static and MAS spectra, they are clearly revealed in the DOR spectrum, where they give rise to an anisotropic broadening and different isotropic shifts for each satellite transition. The residual third-order anisotropy in DOR is expected to be a sixth rank tensor, which, in principle, can be eliminated by adding a third rotation about an angle of 21.18°, that is, the root of $P_6(\cos\theta_3)$, where θ_3 is the third rotation angle. While not experimentally possible, we tested this hypothesis by simulating the triple rotation spectrum also shown in Fig. 6, and, as predicted, the residual anisotropy in the DOR spectra is eliminated, and an isotropic spectrum was obtained.

Finally, we note that for nuclei experiencing the same

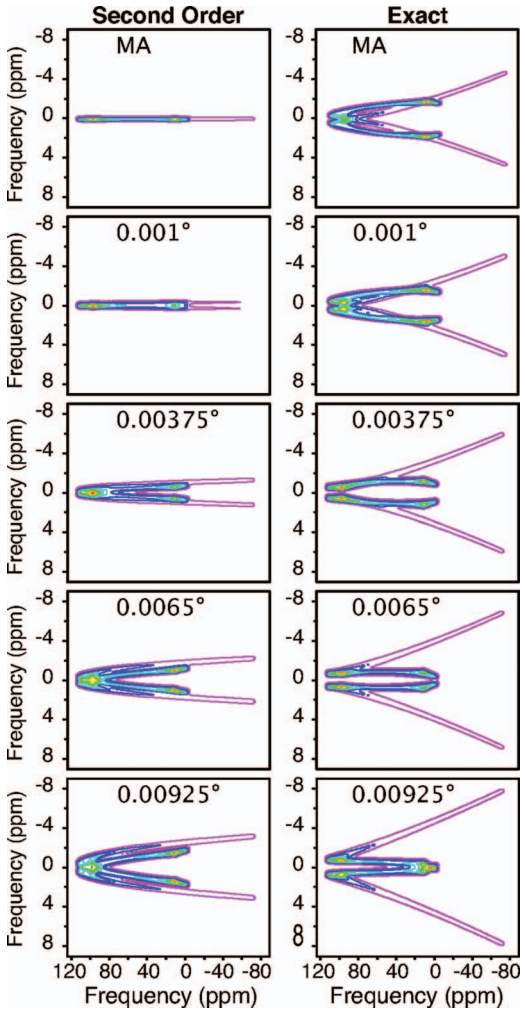

FIG. 5. (Color) Comparison of 2D ST-MAS spectra at various angles away from the magic-angle and at different levels of theory. In the left column are ST-MAS spectra simulated using second-order eigenvalues with zeroth-order eigenstates. In the right column are ST-MAS spectra simulated using exact eigenvalues with zeroth-order eigenstates. At the top in both columns are the simulated ST-MAS spectra spinning at magic-angle. Moving down from the top in both columns are ST-MAS spectra obtained at angles slightly away from the magic angle. NMR parameters for Andalusite used in the simulation were C_q=15.3 MHz and η_q=0.13.

electric field gradient the size of the quadrupolar coupling Hamiltonian increases in magnitude with the nuclear quadrupole moment, which, in turn, decreases with increasing spin I [see Eq. (34)]. This makes spin $I=1$ nuclei the most susceptible to higher-order quadrupolar effects in NMR. Recent experiments by Gan[16] and Bodenhausen and co-workers[17–19] have demonstrated, with accurate magic-angle adjustment,[39] that it is feasible to obtain single ^{14}N MAS spectra in solids using indirect detection of the ^{14}N signal via a directly attached spin 1/2 nucleus, such as ^{13}C (Refs. 16–18) or ^{1}H.[19] In such experiments, our simulations (shown in Fig. 7), indicate that quite noticeable third-order effects will be present for ^{14}N nuclei having moderate values of C_q, even at field strengths as high as 18.8 T. Comparing the spectra calculated with second-order eigenvalues to those with exact eigenvalues one sees that the third-order correction causes a lifting of the degeneracy for the $m=-1\rightarrow 0$ and $m=0\rightarrow 1$ transition under MAS. The overlapping powder

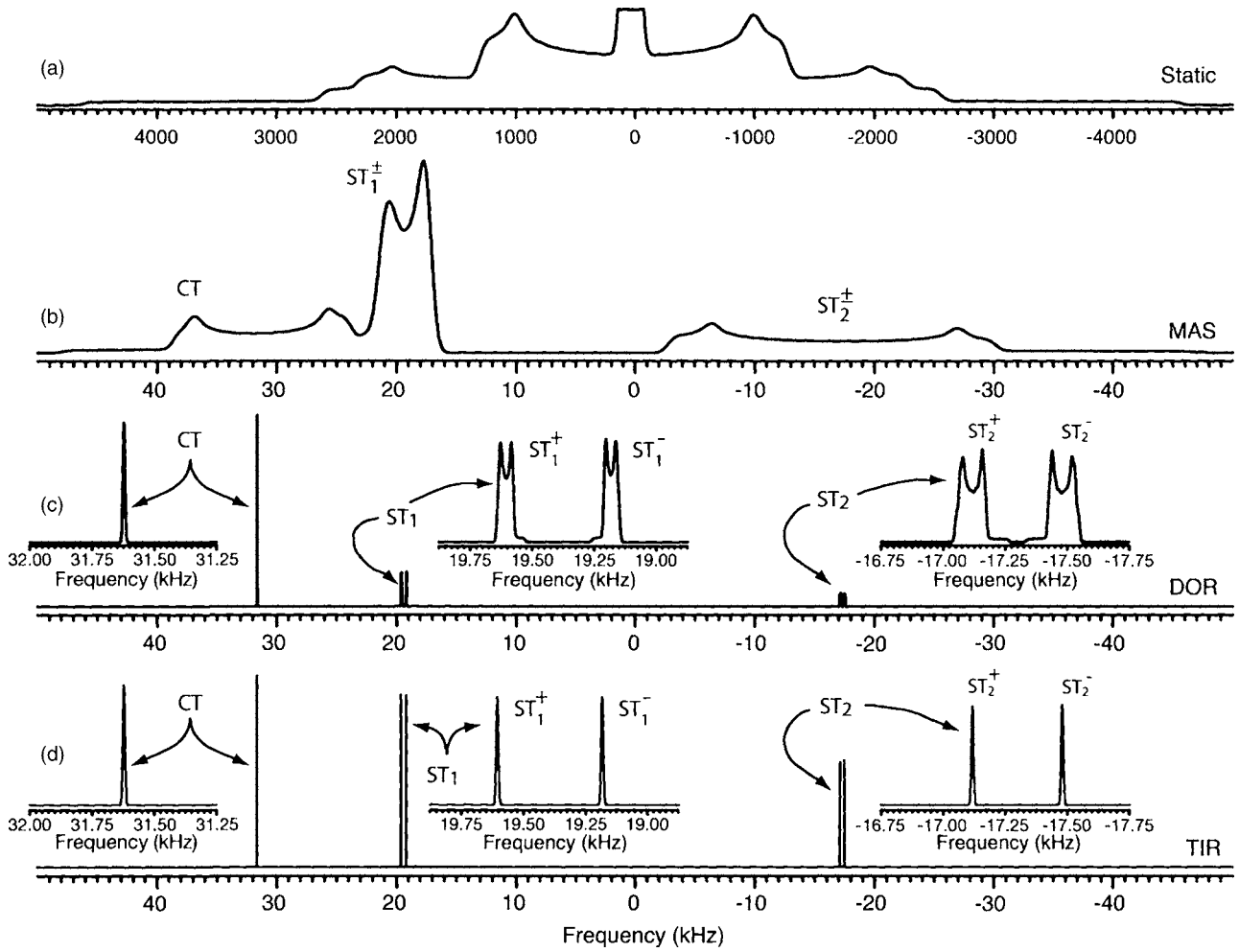

FIG. 6. Comparison of static, magic-angle spinning, double rotation, and triple rotation simulated spectra of ^{27}Al NMR in Andalusite at 11.7 Tesla with C_q=15.3 MHz and η_q=0.13. In (b) the MAS spinning speed was 100 kHz. In (c) the DOR outer rotor angle and speed were 54.74° and 100 kHz, respectively, and the inner rotor angle and speed was 30.56° and 500 kHz. In (d) the triple rotation (TIR) outer rotor angle and speed were 54.74° and 100 kHz, respectively, the middle rotor angle and speed were 30.56° and 700 kHz, respectively and the innermost rotor angle and speed were 21.18° and 4900 kHz, respectively. Calculations were performed using exact eigenvalues and zeroth-order eigenvectors.

patterns for these two transitions will lead to a more complex lineshape than what is predicted from second-order perturbation only, and could be misinterpreted as multiple sites where there is only one. Clearly, such higher-order effects will need to be taken into account for any detailed analysis of such spectra.

V. SUMMARY

We have described a general theoretical approach for including higher-order effects in a full density matrix treatment of a multiple-pulse, sample rotation experiment on a arbitrary nucleus of spin I. This approach first requires identifying the frame where the stationary state Hamiltonian is diagonal. The orientation of this frame with respect to the laboratory frame will depend on the individual crystallite orientation. After transforming the excitation and observable operators from the laboratory into diagonal frame we perform a generic expansion of these "tilted" operators using unit irreducible tensor operators. When taken into the "rotating tilted" frame, which rotates about the z-axis of the diagonal frame, the irreducible tensor operator expansion is decomposed in terms of harmonics of the fundamental Zeeman frequency. This decomposition facilitates an analytical filtering of the observable and the excitation Hamiltonian to obtain versions which focus on a specific band of transitions. We also include a treatment of higher-order effects during sample rotation, employing the adiabatic approximation and taking care to correct for quantum mechanical anholonomy that can arise with time-dependent eigenstates.

Using the examples of overtone NMR and nonsymmetric transitions of quadrupolar nuclei, we apply a numerical implementation of this theoretical approach. Simulations of ^{14}N overtone NMR reveal an excitation offset dependence that is quite severe at external static field strengths B_0 and low rf excitation field strengths B_1. Additionally, sample rotation was shown to have a devastating effect on overtone sensitivity. This effect arises from a mismatch between a crystallite orientation dependent effective phase of the receiver coil and a crystallite orientation dependent effective phase of the rf excitation in the overtone experiment.[26] Even though DOR has the ability to eliminate frequency anisotropies in ^{14}N overtone NMR, the mismatch of effective phases during sample rotation leads to such a dramatic signal loss that its usefulness is questionable. Finally, we show that re-

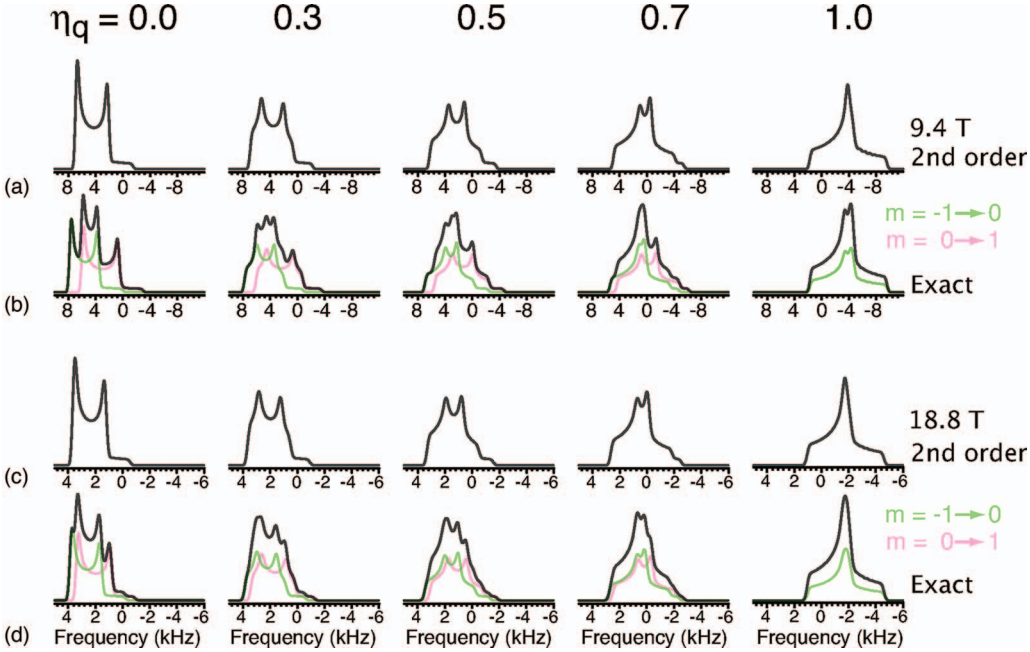

FIG. 7. (Color) Comparison of rotor synchronous ^{14}N MAS single quantum spectra using (a) second-order eigenvalues and (b) exact eigenvalues at 9.4 T and (c) second-order eigenvalues and (d) exact eigenvalues at 18.8 Tesla. For all simulations C_q=3 MHz was used. The η_q values are indicated above. Additional simulation parameters: $\omega_R/2\pi$=40 000 Hz, and dwell time=25 μs. Calculations were performed using exact eigenvalues and zeroth-order eigenvectors.

cent observations of third-order effects in solid-state NMR spectra are well described by this approach, and with this improved understanding solid-state NMR spectra can now be properly interpreted for sample characterization.

ACKNOWLEDGMENTS

One of the authors (P.J.G.) acknowledges Alex Pines for helpful discussions on the adiabatic approximation and Zhehong Gan and Geoffrey Bodenhausen for helpful discussions on indirect detection of ^{14}N MAS NMR. This material is based upon work supported in part by the National Science Foundation under Grant No. CHE-0616881 and Le Studium, Orlèans, France. Any opinions, findings and conclusions or recommendations expressed in this material are those of the author(s) and do not necessarily reflect the views of the National Science Foundation (NSF).

APPENDIX A: TRANSFORMING I_X AND I_Z INTO THE DIAGONAL FRAME

To improve the efficiency of numerical simulations we take advantage of selection rules to eliminate summations over matrix elements that are zero. Starting with

$$Z_{l,m} = (-1)^m \mathrm{Tr}(\mathbf{V}^\dagger \mathbf{I}_Z \mathbf{V} \mathcal{T}_{l,-m}) = (-1)^m \sum_{r,s,t,u} \langle s|\mathbf{V}^\dagger|r\rangle\langle r|\mathbf{I}_Z|u\rangle\langle u|\mathbf{V}|t\rangle\langle t|\mathcal{T}_{l,-m}|s\rangle, \quad \text{(A1)}$$

we can apply the general selection rule for irreducible tensors,

$$\langle t|\mathcal{T}_{l,-m}|s\rangle = \delta_{t,s-m}\langle s-m|\mathcal{T}_{l,-m}|s\rangle, \quad \text{(A2)}$$

to restrict the sum over t to the cases where $t=s-m$. These rules applied to $\langle r|\mathbf{I}_Z|u\rangle$ further restricts the sum of u to the cases where $u=r$. Combining these with $\langle s|\mathbf{V}^\dagger|r\rangle=\langle r|\mathbf{V}|s\rangle^*$ leaves

$$Z_{l,m} = (-1)^m \sum_{r,s} \langle r|\mathbf{V}|s\rangle^* \langle r|\mathbf{I}_Z|r\rangle\langle r|\mathbf{V}|s-m\rangle\langle s-m|\mathrm{T}_{l,-m}|s\rangle. \quad \text{(A3)}$$

Using similar arguments one also obtains

$$X_{l,m} = \frac{(-1)^m}{2} \sum_{r,s} \big[\langle r|\mathbf{V}|s\rangle^* \langle r|\mathbf{I}_+|r-1\rangle\langle r-1|\mathbf{V}|s-m\rangle\langle s - m|\mathrm{T}_{l,-m}|s\rangle + \langle r|\mathbf{V}|s\rangle^* \langle r|\mathbf{I}_-|r+1\rangle\langle r+1|\mathbf{V}|s-m\rangle\langle s - m|\mathrm{T}_{l,-m}|s\rangle\big]. \quad \text{(A4)}$$

APPENDIX B: $X_{l,m}$ AND $Z_{l,m}$ PERTURBATION EXPANSIONS

The $X_{l,m}$ and $Z_{l,m}$ can be expanded in the following perturbation series:

$$X_{l,m} = X^{(0)}_{l,m} + X^{(1)}_{l,m} + \cdots, \quad \text{(B1)}$$

$$Z_{l,m} = Z^{(0)}_{l,m} + Z^{(1)}_{l,m} + \cdots. \quad \text{(B2)}$$

and each term was obtained from the perturbation expansion of $\mathbf{V}$. In a static perturbation analysis to zeroth-order for eigenvectors we have $\mathbf{V}=1$, and one finds that all $X^{(0)}_{l,m}$ and $Z^{(0)}_{l,m}$ are zero except

$$X^{(0)}_{1,m} = -\frac{m f^{(0)}_I}{\sqrt{2}} \quad \text{and} \quad Z^{(0)}_{1,0} = f^{(0)}_I. \quad \text{(B3)}$$

Considering the quadrupolar interaction as perturbation to the Zeeman interaction, the first order correction to $\mathbf{V}$ is

$$\mathbf{V}^{(1)} = \frac{\omega_q}{\omega_0} \sum_{m \neq 0} (-1)^m \frac{A_{2,-m}(\Omega_q)\mathbf{T}_{2,m}}{m}. \tag{B4}$$

With this expression one finds that the first-order corrections $X^{(1)}_{l,m}$ and $Z^{(1)}_{l,m}$ are zero except

$$X^{(1)}_{2,0} = \frac{\omega_q}{\omega_0} f_I^{(0)} f_I^{(1)} \left[-\sqrt{\frac{3}{2}} (A_{2,-1}(\Omega_q) - A_{2,1}(\Omega_q)) \right],$$

$$X^{(1)}_{2,\pm 1} = \frac{\omega_q}{\omega_0} f_I^{(0)} f_I^{(1)} \left[\pm \frac{A_{2,\mp 2}(\Omega_q)}{2} \right], \tag{B5}$$

$$X^{(1)}_{2,\pm 2} = \frac{\omega_q}{\omega_0} f_I^{(0)} f_I^{(1)} [\mp A_{2,\mp 1}(\Omega_q)],$$

and

$$Z^{(1)}_{2,m\neq 0} = \frac{\omega_q}{\omega_0} f_I^{(0)} f_I^{(1)} [(-1)^m A_{2,-m}(\Omega_q)]. \tag{B6}$$

[1] A. Samoson, E. Lippmaa, and A. Pines, Mol. Phys. **65**, 1013 (1988).
[2] B. F. Chmelka, K. T. Mueller, A. Pines, J. Stebbins, Y. Wu, and J. W. Zwanziger, Nature (London) **339**, 42 (1989).
[3] K. T. Mueller, B. Q. Sun, G. C. Chingas, J. W. Zwanziger, T. Terao, and A. Pines, J. Magn. Reson. **86**, 470 (1990).
[4] L. Frydman and J. S. Harwood, J. Am. Chem. Soc. **117**, 5367 (1995).
[5] A. Medek, J. S. Harwood, and L. Frydman, J. Am. Chem. Soc. **117**, 12779 (1995).
[6] Z. Gan, J. Am. Chem. Soc. **122**, 3242 (2000).
[7] F. Wolf, D. Kline, and H. S. Story, J. Chem. Phys. **53**, 3538 (1970).
[8] Z. Gan, P. Srinivasan, J. R. Quine, S. Steuernagel, and B. Knott, Chem. Phys. Lett. **367**, 163 (2003).
[9] A. Bain, Mol. Phys. **101**, 3163 (2003).
[10] D. Iuga, C. Morais, Z. Gan, D. R. Neuville, L. Cormier, and D. Massiot, J. Am. Chem. Soc. **127**, 11540 (2005).
[11] M. Deschamps, F. Fayon, V. Montouillout, and D. Massiot, Chem. Commun. (Cambridge) **2006**, 1924.
[12] S. Wi and L. Frydman, J. Chem. Phys. **112**, 3248 (2000).
[13] S. Wi, V. Frydman, and L. Frydman, J. Chem. Phys. **114**, 8511 (2001).
[14] S. Wi, S. E. Ashbrook, S. Wimperis, and L. Frydman, J. Chem. Phys. **118**, 3131 (2003).
[15] H. T. Kwak, P. Srinivasan, J. Quine, D. Massiot, and Z. Gan, Chem. Phys. Lett. **376**, 75 (2003).
[16] Z. H. Gan, J. Am. Chem. Soc. **128**, 6040 (2006).
[17] S. Cavadini, A. Lupulescu, S. Antonijevic, and G. Bodenhausen, J. Am. Chem. Soc. **128**, 7706 (2006).
[18] S. Cavadini, S. Antonijevic, A. Lupulescu, and G. Bodenhausen, ChemPhysChem **8**, 1363 (2007).
[19] S. Cavadini, S. Antonijevic, A. Lupulescu, and G. Bodenhausen, J. Magn. Reson. **182**, 168 (2006).
[20] M. Goldman, P. J. Grandinetti, A. Llor, Z. Olejniczak, J. R. Sachleben, and J. W. Zwanziger, J. Chem. Phys. **97**, 8947 (1992).
[21] R. Tycko and S. J. Opella, J. Chem. Phys. **86**, 1761 (1987).
[22] P. J. Grandinetti, Solid State Nucl. Magn. Reson. **23**, 1 (2003).
[23] M. H. Levitt, J. Magn. Reson. **126**, 164 (1997).
[24] G. J. Bowden and W. D. Hutchison, J. Magn. Reson. **67**, 403 (1986).
[25] D. I. Hoult and R. E. Richards, J. Magn. Reson. **24**, 71 (1976).
[26] L. Marinelli, S. Wi, and L. Frydman, J. Chem. Phys. **110**, 3100 (1999).
[27] M. Eden and M. H. Levitt, J. Magn. Reson. **132**, 220 (1998).
[28] S. K. Zaremba, Ann. Mat. Pura Appl. **4:73**, 293 (1966).
[29] H. Conroy, J. Chem. Phys. **47**, 5307 (1967).
[30] V. B. Cheng, H. H. Suzukawa, and M. Wolfsberg, J. Chem. Phys. **59**, 3992 (1973).
[31] M. Bloom and M. A. LeGros, Can. J. Phys. **64**, 1522 (1986).
[32] R. Tycko and S. J. Opella, J. Am. Chem. Soc. **108**, 3531 (1986).
[33] R. Tycko, P. L. Stewart, and S. J. Opella, J. Am. Chem. Soc. **108**, 5419 (1986).
[34] D. -K.Lee and A. Ramamoorthy, Chem. Phys. Lett. **280**, 501 (1997).
[35] A. Bain, J. Magn. Reson. **179**, 308 (2006).
[36] H. J. Jakobsen, J. Skibsted, H. Bildse, and N. C. Nielsen, J. Magn. Reson. **85**, 173 (1989).
[37] S. E. Ashbrook, S. Antonijevic, A. J. Berry, and S. Wimperis, Chem. Phys. Lett. **364**, 634 (2002).
[38] H. T. Kwak, J. Magn. Reson. **164**, 369 (2003).
[39] S. Antonijevic and G. Bodenhausen, Angew. Chem., Int. Ed. **44**, 2935 (2005).

[40] The Hamiltonian for the coupling of the nuclear electric quadrupolar moment to the surrounding electric field gradient is given by

$$\mathbf{H}_q = \sum_{k=-2}^{2} (-1)^k R_{2,k} \left[\left(\frac{3}{2}\right)^{1/2} \frac{eQ}{I(2I-1)} \mathbf{T}_{2,-k} \right],$$

where $R_{2,k}$ is the electric field gradient tensor at the nucleus and the term inside the square brackets is the nuclear quadrupole moment tensor. With this definition $R_{2,k}$ is an irreducible spherical tensor defined in the laboratory frame, and related to its principal axis system (PAS) values $\rho^{(R)}_{2,k}$ according to

$$R_{2,k} = \sum_{k'=-2}^{2} \mathcal{D}^{(2)}_{k',k}(\Omega) \rho_{2,k'}.$$

In the PAS, $\rho^{(R)}_{2,k'}$ has the values of $\rho^{(R)}_{2,0} = eq/2$, $\rho^{(R)}_{2,\pm 1} = 0$, and $\rho^{(R)}_{2,\pm 2} = \rho^{(R)}_{2,0} \eta_q / \sqrt{6}$, where eq is the expectation value of the electric field gradient (efg) experienced by the nucleus in question, and η_q is the quadrupolar coupling asymmetry parameter. Ω_q are the Euler angles (α, β, γ) between the laboratory frame and the PAS frame. The quadrupolar coupling constant is given by $C_q = e^2qQ/h$ [or $e^2qQ/(4\pi\epsilon_0 h)$ in SI units]. Often for convenience, however, a different irreducible spherical tensor $A_{2,k}$, related to $R_{2,k}$ by

$$A_{2,k} = \left(\frac{3}{2}\right)^{1/2} \frac{\hbar}{eq} R_{2,k}$$

is used. Here $\rho^{(A)}_{2,0} = 1/\sqrt{6}$ and $\rho^{(A)}_{2,\pm 2} = \rho^{(A)}_{2,0} \eta_q / \sqrt{6}$. Then we rewrite the quadrupolar Hamiltonian as given in Eq. (33).